Stability Analysis of Multi-line Parallel Tunnels Underpassing Existing Sloping Tunnels

Wei Zhang

CISPDR Corporation, Wuhan, China
Email: zhangwei@cjwsjy.com.cn

Abstract. With the rapid development of urbanization and transportation, the demand for tunnel engineering in complex terrains is growing. Multi-line parallel tunnels passing through existing ones present significant technical challenges due to their unique structure and complex construction environment. This study evaluates the stability of the multi-line inclined tunnel in the Dongfeng Mountain Tunnel (National Highway G316) using numerical simulation. The Mohr-Coulomb yield criterion was applied to simulate the impact of tunnel excavation on surrounding rock stress, displacement, and stability, as well as the safety of the support structure. Results show the maximum principal compressive stress of the surrounding rock is 5.73 MPa, lower than its uniaxial saturated compressive strength. The new tunnel's arch settlement is 6.83 mm, with a maximum horizontal displacement of 1.39 mm. The existing tunnel experiences a maximum settlement of 3.30 mm on the left and 3.47 mm on the right. Local tensile-stress concentrations indicate potential cracking-prone locations during the initial support phase, requiring reinforcement and monitoring. The research provides a preliminary numerical reference for multi-line parallel tunnels intersecting existing ones, supporting the preliminary construction design and safety assessment of similar projects under comparable geological and construction conditions.

Keywords: Multi-line parallel, stability of tunnel surrounding rock, stress; displacement, initial support

1 Introduction

With the rapid growth of urbanization and transportation networks, the demand for tunnel construction in complex terrain conditions continues to rise. Multi-line parallel tunnel projects that intersect existing tunnels have become a significant technical challenge in tunnel engineering due to their unique structural form and complex construction environment (Zheng *et al*., 2025) [7-8]. Unlike single-tunnel or horizontal/vertical intersecting projects, multi-line parallel tunnels underpassing inclined existing tunnels involve complex spatial interactions: the inclined orientation of the existing tunnel changes the stress distribution of the surrounding rock, while the parallel arrangement of new tunnels exacerbates mutual interference during excavation. These factors can lead to unforeseen risks, such as uneven settlement of existing tunnels, local cracking

© The Author(s) 2026
H. Wu et al. (eds.), *Proceedings of the 2026 3rd International Conference on Civil Engineering Structures and Concrete Materials (CESCM 2026)*, Advances in Engineering Research 312,
https://doi.org/10.2991/978-94-6239-865-8_16

of surrounding rock, or failure of support structures, which are not adequately addressed in current engineering practices.

In recent years, scholars both domestically and internationally have conducted research on the construction of tunnels beneath existing ones or multi-line parallel tunnels. Ma *et al*. (2014) [2] proposed a new method for calculating ground loss in horizontally arranged double tunnels based on the Peck formula, offering valuable reference for future urban railway projects of a similar nature. The model indicates that the shape of the settlement troughs above the twin tunnels is influenced by the sequence of tunnel excavation. Settlement occurs due to the coupled effects of the existing tunnel and the newly excavated tunnel. Zeng *et al*. (2016) [6] proposed an analytical solution for soil deformation caused by double circular shield tunneling construction, predicting and analyzing surface settlement and horizontal deformation. A local deformation concentration occurs above the tunnel centre and in the depth. The soil above the tunnel intends to deform towards the centres of the left and right tunnels with an inclination angle of 45°. Ng *et al*. (2016) [3] studied the impact of single tunnel excavation on the stability of surrounding rock in existing tunnels using both experimental and numerical simulation methods. Avgerinos *et al*. (2017) [1] studied the interaction between the construction process of vertically penetrating existing tunnels and tunnel structures, discussing the effects of circumferential forces, bending moments, and lining on the stability of existing tunnels. During the excavation of the new tunnel, the presence of the existing tunnel influences the rate at which cross-sectional settlement develops in its vicinity. It is also recognized that the surface settlement is jointly governed by the interaction between the existing tunnel and new tunnel. Wu *et al*. (2022) [5] analyzed the mechanical behavior of multi-line parallel tunnels using numerical simulation methods and explored the influence of tunnel spacing on the stress in surrounding rock. These studies provide an important theoretical foundation and practical insights for multi-tunnel parallel tunnel engineering that intersects existing tunnels. Existing studies have laid a foundation for tunnel underpass engineering, but critical gaps remain. First, most research focuses on horizontal double tunnels (Ma et al., 2014 [2]) or vertical intersections (Avgerinos et al., 2017 [1]), with limited attention to inclined existing tunnels—where the angle between new and existing tunnels introduces asymmetric stress and displacement responses that differ from horizontal/vertical cases. Second, studies on multi-line parallel tunnels (Wu et al., 2022 [5]) primarily investigate the influence of tunnel spacing on surrounding rock stress but ignore the coupling effect between inclined existing tunnels and multi-line new tunnels, especially under deep-buried (≈300 m) and complex lithological conditions (slightly weathered tuffaceous lava). Third, analytical solutions for soil deformation (Zeng et al., 2016 [6]) and experimental studies on single-tunnel underpasses (Ng et al., 2016 [3]) cannot fully capture the dynamic interaction between multiple new tunnels and an inclined existing tunnel during step-by-step excavation.

To address these gaps, this study takes the Dongfeng Mountain Tunnel (National Highway G316) as a case study, where four new parallel tunnels (two main roads + two auxiliary roads) underpass an existing inclined tunnel at a 64° plane angle. Numerical simulations were conducted using the Mohr-Coulomb yield criterion to analyze the redistribution of stress, displacement characteristics, and stability of the surrounding

rock, as well as to assess the safety of the initial support structures. The objectives are to: (1) characterize the numerical interaction response between multi-line parallel new tunnels and an inclined existing tunnel; (2) quantify the displacement and stress responses of both new and existing tunnels under the adopted modeling assumptions; and (3) provide technical information for reinforcement and monitoring during construction. This research provides a case-based numerical analysis of an inclined underpass scenario and offers a reference for similar complex tunnel projects.

2 Background

The Changle Zhanggang to Yingqian section of National Highway G316 features a 4-hole separated structure, with the four tunnels intersecting the Dongfeng Mountain Tunnel in the southeast section of the Fuzhou Ring Road under construction at a plane angle of approximately 64°. The vertical clearance between the two tunnels ranges from 24 m to 28 m, with the underpass area buried at a depth of approximately 300 m. It is situated in a slightly weathered tuffaceous lava formation, with a ground elevation ranging from 25m to 420 m, resulting in a relative height difference of about 395 m. The tunnel features a central dual-hole, eight-lane main road tunnel, with dual-hole, two-way, four-lane auxiliary road tunnels on each side. The clearance between adjacent tunnels exceeds 25 m. The main road tunnel has a maximum excavation span of 20.21 m and a height of 13.81 m, while the auxiliary road tunnel spans 12.18 m with a height of 10.03 m. The tunnel section is shown in Figure 1.

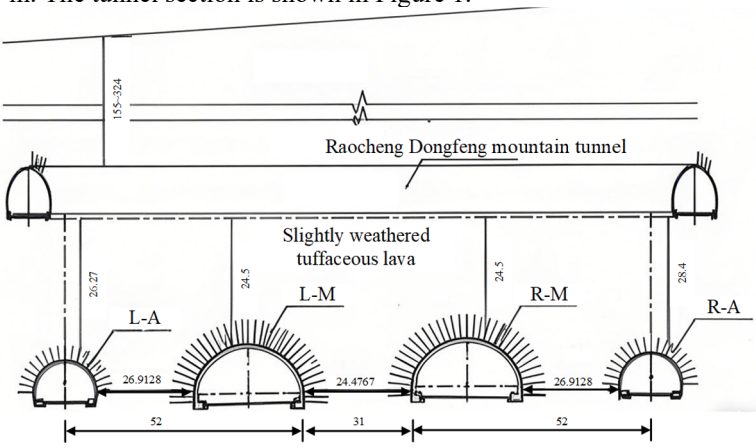


Fig. 1. Schematic diagram of tunnel section (Units: m). L-A, L-M, R-M, and R-A represent the left auxiliary tunnel, left main tunnel, right main tunnel, and right auxiliary tunnel, respectively, while L-E and R-E denote the existing left and right tunnels.

Unlike typical tunnels, when one tunnel passes beneath an existing one, soil disturbance or inadequate support structures can lead to ground subsidence, compromising the stability of both the existing tunnel and the surrounding structures above. Furthermore, constructing new tunnels may impose additional loads and stresses

on the existing ones, particularly when the structural distance between them is minimal, potentially causing safety hazards such as structural instability and crack propagation in the existing tunnel (Zheng *et al*., 2025) [8]. When an angle exists between an existing tunnel and a newly constructed one, the interaction between them becomes more complex. Therefore, it is essential to understand the response mechanisms of multi-line tunnel construction beneath inclined multi-line tunnels, providing scientific guidance for on-site design and safety assessment.

3 Response of Underpassing Existing Tunnels

The study area primarily consists of slightly weathered tuffaceous lava. According to the available engineering geological investigation, the rock mass in the underpassing zone is relatively intact, and no distinct directional joints were identified within the modeled zone. However, detailed quantitative data regarding joint orientation, spacing, persistence, and aperture were not available for the present numerical analysis. Owing to its low permeability, no seepage pressure was detected during field investigations. Because the present study focuses on the overall interaction between the existing and newly constructed tunnels, the rock mass was assumed to be a homogeneous and isotropic equivalent continuum, and the influence of groundwater was neglected. This assumption represents a modeling simplification and does not imply that discontinuities have no influence on local rock-mass behavior. The Mohr-Coulomb yield criterion is applied to analyze the stress and displacement of the tunnel structure (Troncone *et al*., 2022) [4]. The specific calculation parameters are provided in Table 1.

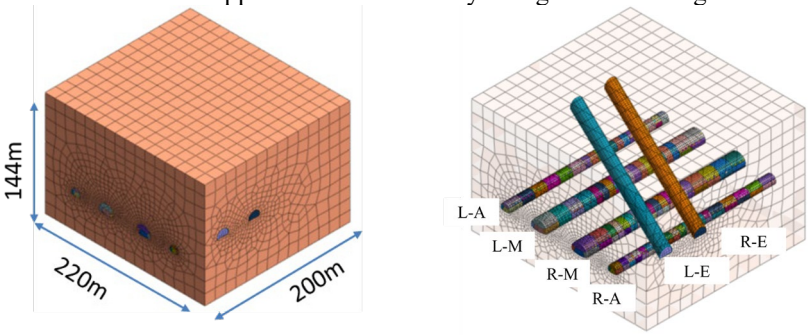
Table 1. Calculation parameters.

Material	Elastic modulus (Gpa)	Poisson's ratio	Density (Kg/m^3)	Internal friction angle (°)	cohesion (MPa)
Slightly weathered tuffaceous lava	11	0.26	2500	44	1.1
Auxiliary tunnel initial support	25.3	0.2	2300	/	/
Main tunnel initial support	25.5	0.2	2300	/	/
Secondary lining	31.5	0.2	2500	/	/

The parameters listed in Table 1 were used as equivalent rock-mass parameters at the numerical-model scale. The Mohr-Coulomb model was adopted because the present study focuses on the overall stress redistribution and deformation interaction of the multi-tunnel system during staged excavation. Nevertheless, this model cannot explicitly reproduce brittle damage, post-peak strain softening, anisotropic joint-controlled deformation, or tensile crack propagation. Therefore, the calculated tensile-stress zones

are interpreted as potential damage-prone locations rather than as direct predictions of crack initiation or propagation. More advanced constitutive models, such as the Hoek-Brown or strain-softening models, may produce different stress and plastic-zone magnitudes and should be examined when more complete rock-mass data become available.

Since tunnel excavation typically impacts the surrounding rock within a range of 3 to 5 times the tunnel diameter, the model dimensions were set at 220m in length, 200m in width, and 144m in height, to reduce the influence of the model boundaries on the calculated response. The initial support of the newly built tunnel is modeled using plate elements, with the secondary lining temporarily excluded. Research indicates that both the existing and new tunnels exert a collective influence on surface settlement (Ma *et al*., 2014 [2]; Avgerinos *et al*., 2017 [1]). Consequently, it is essential to account for the effects of both the initial support and the secondary lining in the existing tunnel.



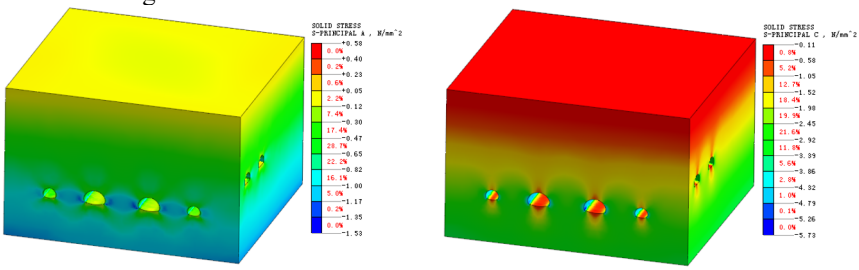
(a) Model dimension (b) Model perspective view

Fig. 2. Computation model.

Regarding boundary conditions, all surfaces, except the model's top, were subjected to normal displacement constraints. Only the effect of self-weight was considered in the calculation. This treatment provides a simplified representation of the in-situ stress field associated with the approximately 300 m overburden. Therefore, the numerical results are primarily used to evaluate relative stress redistribution and deformation trends rather than to reproduce the complete regional stress field. The calculation model is shown in Figure 2. The numerical simulation sequence comprised three primary stages: (1) in-situ stress equilibration; (2) simultaneous excavation and support of existing tunnels; and (3) excavation and support of new tunnels. The excavation of new tunnels followed a specific sequence: the left and right auxiliary tunnels were excavated first, followed by the left main tunnel, and finally the right main tunnel.

The calculation simulates the prescribed tunnel excavation and initial support construction process, including the gradual release of excavation load during construction. During excavation, the released load is shared by the surrounding rock and initial support. At the end of excavation, 40% of the load is released, with an additional 30% released after the initial support was completed. Thus, the reported results correspond to the adopted construction stage rather than to a fully released final state. The load-release percentages were used as simplified numerical representations of the excavation-support process, and their influence should be considered when interpreting the

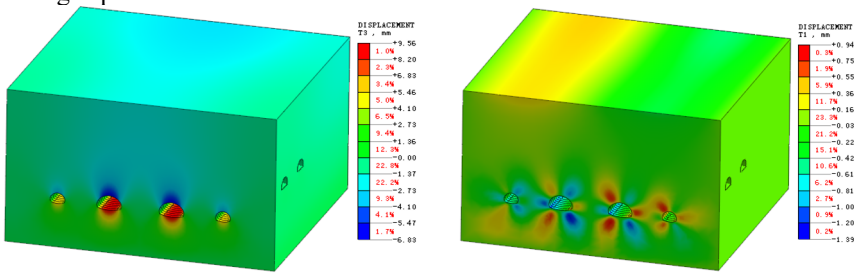
calculated stress magnitudes. Figure 3 shows the first and third principal stresses of the surrounding rock at the last modeled construction step. The maximum tensile stress was 0.58 MPa, and the maximum compressive stress was 5.73 MPa. The maximum compressive stress was lower than the saturated uniaxial compressive strength of slightly weathered tuff (85 MPa) reported in the geological survey. However, the tensile stress cannot be evaluated using the uniaxial compressive strength, and the adopted constitutive model does not explicitly simulate tensile crack propagation. Therefore, the tensile-stress result is used only to identify potential tensile-damage-prone zones. Combined with the calculated displacement response, these results indicate a generally controlled global response under the adopted assumptions, rather than demonstrating that local rock-mass damage cannot occur.



(a) First principal stress (b) Third principal stress

Fig. 3. Main stress cloud map of surrounding rock after step-by-step excavation of tunnel.

Figure 4 shows the displacement cloud map after the new tunnel excavation simulation. The maximum vertical displacement occurs at the arch crown of the two main tunnels, with a settlement of 6.83 mm, while the maximum horizontal displacement is at the left and right side walls, reaching 1.39 mm. The model results align closely with the design specifications.



(a) Vertical displacement (b) Horizontal displacement

Fig. 4. Cloud map of surrounding rock displacement after step-by-step excavation of tunnel.

The deformation of the surrounding rock is characterized by a coupled mode, dominated by the new large-span main tunnels. This mode features pronounced crown settlement accompanied by lateral convergence at the haunches and sidewalls, resulting in an ovalization of the tunnel cross-section. The formation of the settlement peak above

the main tunnels can be attributed to their larger span, which induces the most intense stress release in the crown region during excavation and leads to the widest zone of equivalent stiffness degradation. Consequently, vertical convergence preferentially localizes at the crown and propagates upward (Figure 4(a)). In contrast, the auxiliary tunnels, with smaller spans, exert a relatively limited influence on the vertical displacement field. The horizontal displacement distribution (Figure 4(b)) reflects radial convergence of the surrounding rock toward the tunnel cavities. The maximum horizontal displacement is observed at the left and right sidewalls. Near the springline, the convergence direction is closer to horizontal, which results in a significantly larger horizontal component of displacement. In contrast, radial convergence at the crown primarily manifests as vertical displacement. The magnitude of horizontal displacement is markedly reduced in the rock pillars between adjacent tunnels, which can be attributed to the superposition of convergence fields from adjacent tunnels and the additional confinement provided by the intervening rock mass under multi-tunnel conditions, thereby weakening the net lateral displacement.

Step-by-step excavation leads to pronounced redistribution of the surrounding-rock principal stresses around the excavation boundary (Figure 3), with stress release and stress reorganization being most evident in the crown and haunch regions. This excavation-induced stress adjustment causes the local stress state to evolve from one dominated by compressive stresses to a coupled compression–unloading condition, providing the stress-mechanical basis for the deformation characteristics identified (Figure 4). It also explains the occurrence of tensile stress zones at the haunches of the initial support. Figure 4 indicates that during the construction stage the initial support does not behave as an ideal purely compressive arch, but instead undergoes a distinct ovalization deformation. This deformation introduces bending effects into the support ring, causing bending moments to concentrate at the haunches and corner regions where curvature and restraint conditions change abruptly, thereby driving one side of the lining thickness into tension. As a result, tensile stress concentration is more likely to develop at the haunches of the large-span main tunnels, making these locations potential cracking zones. These tensile stress zones are mechanically consistent with the excavation-induced principal stress redistribution (Figure 3) and the ovalization-type deformation mode inferred from the displacement fields (Figure 4). Nevertheless, because crack initiation and post-cracking behavior were not explicitly simulated, these zones indicate potential cracking-prone locations rather than confirmed cracking.

Figure 5 and Figure 6 respectively show the vertical displacement and floor settlement curves of the existing line tunnel. The construction of the new tunnels has impacted the settlement of existing lines. The maximum settlement occurs above the top of the new tunnel's main tunnel, with the left tunnel settling 3.30 mm and the right tunnel settling 3.47 mm. During tunnel excavation, the vertical displacement impact is minimal when the excavation is far from the existing line. As the excavation nears the existing line, vertical displacement gradually increases. The rate of change in vertical displacement peaks at the bottom of the existing line. As excavation progresses, the rate of change slows, and the vertical displacement curve stabilizes, as shown in Figure 7.

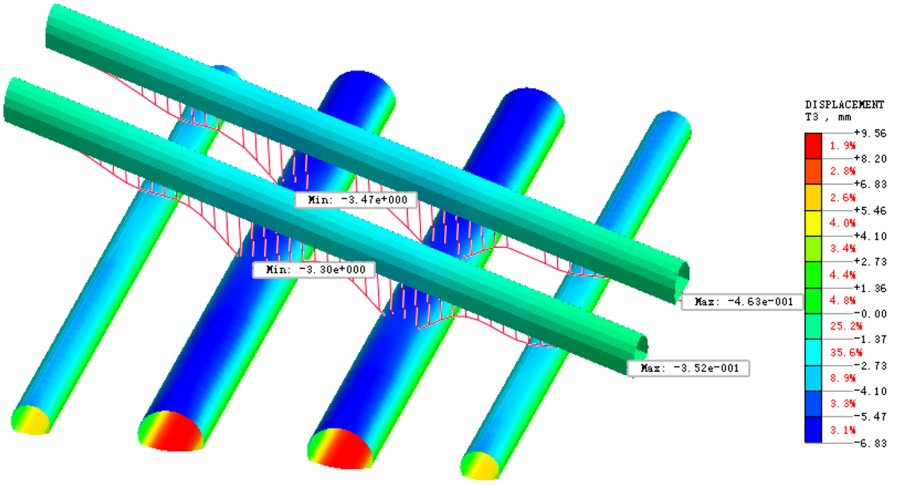


Fig. 5. Cloud map of vertical displacement of tunnels.

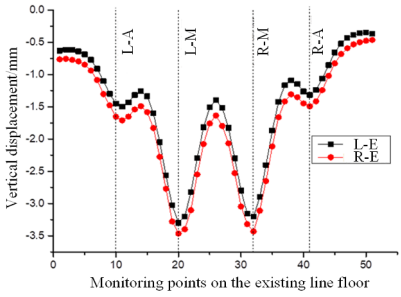


Fig. 6. Settlement curve of existing tunnel floors.

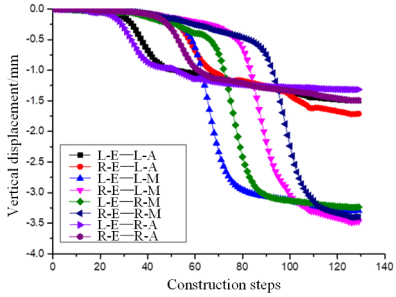


Fig. 7. Influence curve of vertical displacement on the existing tunnel floor caused by the excavation of a new tunnel.

After excavating the new tunnel, the maximum and minimum principal stresses on the initial support structure are shown in Figure 8 and Figure 9. The maximum tensile stress was 9.26 MPa, while the maximum compressive stress was 14.97 MPa. The design uses C25 concrete for the initial support, with an ultimate tensile strength of 2.0 MPa and an ultimate compressive strength of 19.0 MPa. The calculated compressive stress was lower than the nominal compressive strength, whereas the local tensile stress exceeded the nominal tensile strength. These results indicate a potential risk of local tensile cracking at the corners on the left and right sides of the main tunnel. Because the plate-element model does not explicitly reproduce crack initiation and post-cracking behavior, the calculated stress exceedance should be interpreted as a risk indicator rather than as a direct prediction of cracking. During construction, reinforcement measures and enhanced monitoring should be implemented to ensure safety.

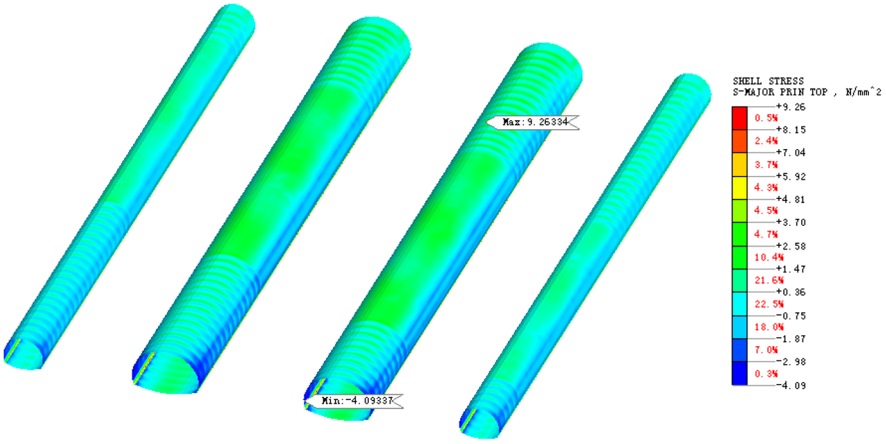


Fig. 8. Cloud map of the maximum principal stress in the initial support of newly excavated tunnels.

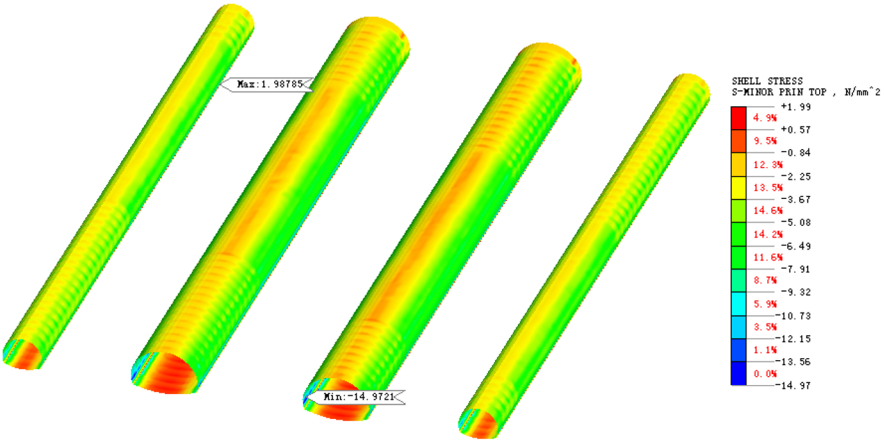


Fig. 9. Cloud map of the minimum principal stress in the initial support of newly excavated tunnels.

4 Conclusions

This study examines the G316 national highway tunnel, focusing on the stability of a multi-tunnel parallel system passing through an existing tunnel, including both the initial support and overall structure. The following conclusions are drawn:

(1) Vertical displacement increases as it approaches the existing tunnel, with the maximum rate of change occurring at the bottom of the existing line. As excavation progresses, the rate of displacement change slows, and the vertical displacement curve gradually stabilizes.

(2) After excavating the new tunnel, the maximum vertical displacement of 6.83 mm occurs at the arch top of the main tunnel, while the maximum horizontal displacement of 1.39 mm is observed at the left and right side walls. The maximum settlement of the existing tunnel occurs above the top of the new tunnel, with a maximum of 3.30 mm on the left line and 3.47 mm on the right line.

(3) The maximum compressive stress of the surrounding rock in the underpass tunnel was below the saturated uniaxial compressive strength of the intact rock, indicating a generally controlled compressive response under the adopted modeling assumptions. The calculated support stresses did not indicate compressive failure, whereas local tensile-stress concentrations suggested a potential risk of cracking at the corners of the left and right side walls of the main tunnel. Reinforcement measures should be implemented during construction, and monitoring should be enhanced to ensure safety. Because joints, brittle fracture, post-peak softening, groundwater pressure, and parameter uncertainty were not explicitly considered, these conclusions apply primarily to the overall stress-redistribution and deformation trends predicted by the present model.

References

1. Avgerinos V, Potts D M and Standing J R 2017 Numerical investigation of the effects of tunnelling on existing tunnels *Geotechnique* **67**(9) pp 808-822.
2. Ma L, Ding L and Luo H 2014 Non-linear description of ground settlement over twin tunnels in soil *Tunnelling and Underground Space Technology* **42** pp 144-151.
3. Ng C W W, Wang R and Boonyarak T 2016 A comparative study of the different responses of circular and horseshoe-shaped tunnels to an advancing tunnel underneath *Geotechnique Letters* **6**(2) pp 168-175.
4. Troncone A, Pugliese L, Parise A and Conte E 2022 A simple method to reduce mesh dependency in modelling landslides involving brittle soils *Geotechnique Letters* **12**(3) pp 1-7.
5. Wu F, He C, Kou H, Wang B, Meng W, Meng H and Guo D 2022 Discussion on Reasonable Clear Spacing of Twin-Tunnels in Weak Surrounding Rock: Analytical Solution and Numerical Analysis *Ksce Journal of Civil Engineering* **26**(5) pp 2428-2442
6. Zeng B, Huang D and He J 2016 Analysis of double-O-tube shield tunnelling-induced soil deformation due to ground loss *Geotechnique Letters* **6**(1) pp 7-15.
7. Zheng P, Tan X, Du Z, et al. 2025 Microscopic damage and deterioration of carbonaceous slate in cold region subjected to freeze-thaw cycles *Journal of Rock Mechanics and Geotechnical Engineering.*
8. Zheng P, Tan X, Xie Y, et al 2025 Study on the tensile strength and fracture characteristics of interlayer mineral grain interfaces in slate exposed to water–rock interaction *Rock Mechanics and Rock Engineering* pp 1-24.

Open Access This chapter is licensed under the terms of the Creative Commons Attribution-NonCommercial 4.0 International License (http://creativecommons.org/licenses/by-nc/4.0/), which permits any noncommercial use, sharing, adaptation, distribution and reproduction in any medium or format, as long as you give appropriate credit to the original author(s) and the source, provide a link to the Creative Commons license and indicate if changes were made.

The images or other third party material in this chapter are included in the chapter's Creative Commons license, unless indicated otherwise in a credit line to the material. If material is not included in the chapter's Creative Commons license and your intended use is not permitted by statutory regulation or exceeds the permitted use, you will need to obtain permission directly from the copyright holder.

